arXiv:1609.08790v1 [physics.optics] 28 Sep 2016

Diffraction coupled phase-locked arrays of quantum cascade lasers with monolithically integrated Talbot cavities

Lei Wang,[1,2,a)] Jin-Chuan Zhang,[2] Zhi-Wei Jia,[2] Yue Zhao,[2] Chuan-Wei Liu,[2] Ying-Hui Liu,[2] Shen-Qiang Zhai,[2] Ning Zhuo,[2] Feng-Qi Liu,[2] and Xian-Gang Xu[1]

[1)] *State Key Laboratory of Crystal Materials, Shandong University, Jinan 250100, People's Republic of China*

[2)] *Key Laboratory of Semiconductors Materials, Institute of Semiconductors, Chinese Academy of Sciences, Beijing 100083, People's Republic of China*

(Dated: 29 September 2016)

Diffraction coupled arrays of quantum cascade laser are presented. The phase-locked behavior is achieved through monolithic integration of a Talbot cavity at one side of the laser array. The principle is based on fractional Talbot effect. By controlling length of Talbot cavity to be a quarter of Talbot distance ($Z_t/4$), in-phase mode operation is selected. Measured far-field radiation patterns reflect stable in-phase mode operation under different injection currents, from threshold current to full power current. Diffraction-limited performance is shown from the lateral far-field, where three peaks can be obtained and main peak and side peak interval is 10.5°. The phase-locked arrays with in-phase mode operation may be a feasible solution to get higher output power and maintain well beam quality meanwhile.

Mid-infrared applications are significant technologies, such as trace gas-sensing, breathe analysis, and free-space optical communications.[1] In this spectra range, quantum cascade lasers (QCLs) are ideal semiconductor coherent light sources because of such features as compact size, room temperature operation, and high reliability.[2,3] However, for traditional narrow ridge QCLs, to force the fundamental mode operation, width of laser active region should be in the order of wavelength, which limits lasers output power. To overcome this problem, many solutions have been reported to achieve stable optical coherence for broad-area devices, including photonic crystal DFB lasers,[4] master-oscillator power-amplifiers,[5] angled cavity lasers,[6] and tilted facet lasers.[7] All these methods have achieved near diffraction-limited beam quality.

Phase-locked arrays technology is another alternative solution, where several numbers of lasers are integrated together coherently.[8] Because the active regions of lasers are separated, such devices have better heat dissipation ability than broad area devices. The key point of phase-locked arrays technology is how to achieve coherence among each laser, which ensures well beam quality. Phase-locked arrays of QCLs with different coupling schemes to achieve coherence have been reported, including evanescent-wave coupled arrays,[9,10] leaky-wave coupled arrays,[11,12] and Y-coupled arrays.[13] The evanescent-wave coupled devices often tend to favor out-of-phase mode, leading to double-lobe far-field patterns;[8] The leaky-wave coupled devices need very complex regrowth process or additional phase sectors to ensure in-phase mode operation;[11,12] Y-coupled devices generally show undesirable self-pulsation dynamics between in-phase and out-of-phase modes due to spatial hole burning effect.[12] Diffraction coupled scheme is another method to phase-lock lasers in an array. In the near-infrared, this method has been successfully employed to achieve phase-locked arrays of semiconductor lasers with diffraction-limited beam quality.[8] In this letter, we expanded the diffraction coupled phase-locked arrays technology into the mid-infrared region with QCLs.

The principle is based on Fractional Talbot effect, which occurs when propagation distance Z of light emitted from a periodic array of light sources satisfies the condition[14]

$$Z = p/q \times Z_t, \tag{1}$$

with

$$Z_t = nd^2/\lambda, \tag{2}$$

where p and q are coprime integers; Z_t is called Talbot distance; n is the index of refraction; d is the spatial period of light sources; λ is the free-space wavelength. In this case, the optical field shows q spaced copies of the origin.

The sketch of the diffraction coupled phase-locked arrays is presented in Figure 1. The emission wavelength of lasers is 4.6 μm. The device consists of a three lasers array and a Talbot cavity. Center-to-center spacing of adjacent lasers is 25 μm, and each laser has a 10-μm-wide (to force fundamental optical mode operation for each individual laser) and 2-mm-long ridge. Because of the existence of Talbot cavity, the optical modes of each laser will couple with each other and generate so called supermodes.[15] The number of supermodes is equal to the number of lasers in the array[15] and the phase difference of each supermode between adjacent lasers is 0 (in-phase), $\pi/2$, and π (out-of-phase) respectively. The in-phase mode is usually desired for practical applications because of better beam quality than others. However, mode competition usually exists between in-phase mode and out-phase mode.[8]

[a)] Electronic mail: wangleimessi@semi.ac.cn

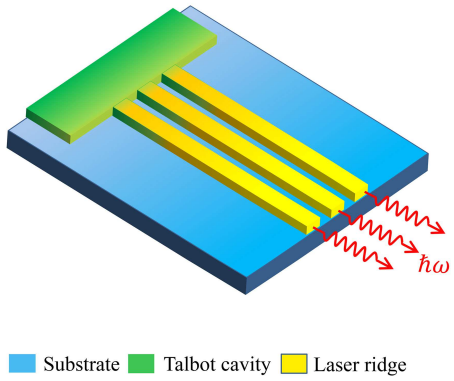

FIG. 1. Sketch of a phase-locked array of QCLs with a integrated Talbot cavity.

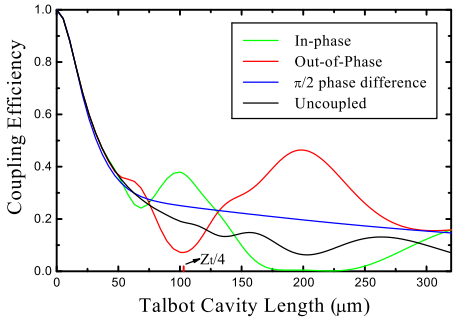

FIG. 2. Coupling efficiencies of different modes versus length of Talbot cavity.

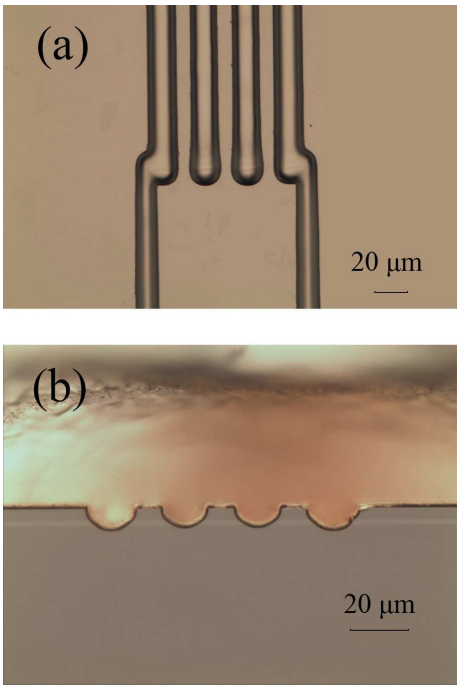

FIG. 3. (a) Optical microscope image of a lasers array and a Talbot cavity after standard photolithographic and wet chemical etching process. (b) Optical microscope cross-sectional image of a phase-locked array of three QCLs.

The supermode selection is related with length of Talbot cavity. After propagating a round trip in Talbot cavity, light will couple into cavity of lasers. The coupling efficiency is dependent on the overlap integral[16]

$$\eta = \frac{\left|\int E(x,y)E_0^*(x,y)dxdy\right|^2}{\int E(x,y)E^*(x,y)dxdy \int E_0(x,y)E_0^*(x,y)dxdy}, \tag{3}$$

where the $E_0(x,y)$ is the initial optical field distribution and the $E(x,y)$ is optical field distribution after propagating a round trip in Talbot cavity. The waveguide losses and mirror losses are nearly no difference for three supermodes or uncoupled mode. Therefore, total optical losses mainly depend on the coupling efficiency at interface of Talbot cavity and lasers cavity. The mode which has the greatest coupling efficiency will have the lowest total optical losses. In other words, such mode operation has the lowest threshold current and is most favored. We simulate relationship between coupling efficiency and length of Talbot cavity. Radiation from each laser source is characterized by a Gaussian beam in plane, where the full waist is regarded as the width of laser ridge (10 μm) and the center-to-center spacing of adjacent sources is 25 μm. The simulated result is shown in Figure 2. When length of Talbot is less than 50 μm, the coupling efficiency of each mode is nearly same, so no mode is favored and then there is no phase-locked behavior. The in-phase mode will have greater coupling efficiency than other modes when length of Talbot cavity is between 75 μm and 125 μm. In this range, the coupling efficiency of in-phase mode reaches the maximum when length of Talbot cavity is near $Z_t/4$, where the index of refraction n to calculate the value of Z_t can be regarded as the effective refraction index N_{eff} in medium. This simulated results fit the theory of fractional Talbot effect.[8,14]Therefore, in order to ensure the in-phase mode operation, we controlled length of Talbot cavity to be $Z_t/4$.

Detailed fabrication process of devices is similar with that of common single-ridge devices.[17] No high-reflectivity or anti-reflectivity coating was applied to each facet. Specially, a scriber with a precision of 5 μm was used to cleaved the wafer into separate devices, to accurately control the length of Talbot cavity to be $Z_t/4$. Fabricated devices is shown in 3.

Pulsed operation was taken at 1.5% duty cycle with 600 ns pulse width for testing. Detailed testing methods are same with Ref. 17. The Figure 4 shows the pulsed operation power versus current (P-I) characteristics. The threshold current is about 1.6 A. Because the total current injection area contains the laser array and the Talbot cavity, the threshold current density (J_{th}) is about 1.9 kA/cm^2. The maximum output optical power is over 350 mw when the injection current is 4.0 A. The measured emission spectrum is shown in the inset of Figure 4. The wavelength peak is 4.6 μm.

What we are most interested in is the far-field radia-

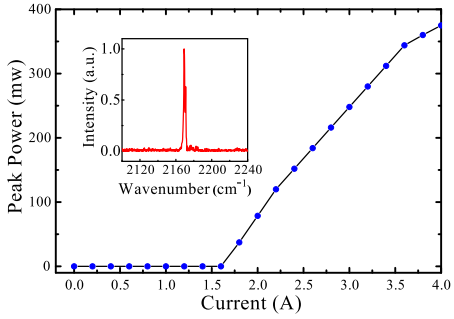

FIG. 4. Output optical power was measured as a function of injection current. The inset is the measured emission spectrum

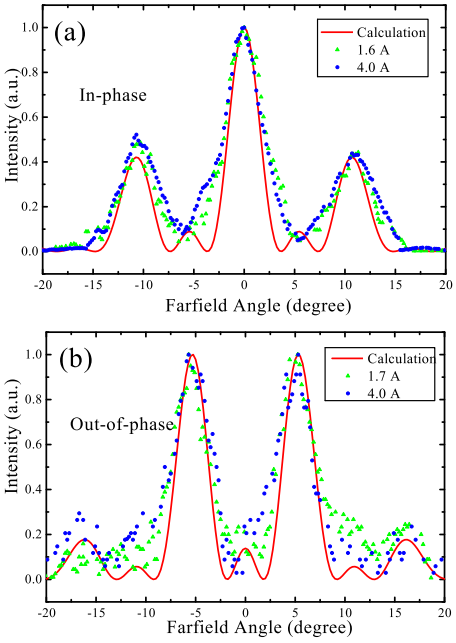

FIG. 5. (a) far-field radiation patterns of device with $Z_t/4$ Talbot cavity length; (b) far-field radiation patterns of device with $Z_t/2$ Talbot cavity length;

tion pattern along the array direction, because it reflects whether phase-locked behavior happens and phase relationship among each laser. Measured lateral far-field radiation patterns of the devices are shown in Figure 4a. The far-field radiation pattern contains three peaks, a central maximum peak and two secondary maximum peaks. The peak with maximum intensity is located at the center with FWHM about 4°. The intensity of secondary maximum peak is approximately 50% of intensity of the central maximum peak and the FWHM of the secondary maximum is also about 4°. The peak separation between the central maximum and the secondary maximum is about 10.5°. Such far-field radiation pattern indicates that near diffraction-limited beam quality is achieved (horizontal beam divergence of 4.6 μm QCLs with 10-μm-width ridge is about 32° for fundamental mode operation).

The multi-peaks shape of normalized far-field profile is a result of optical interference among the light emitted from the three lasers. The multi-slits Fraunhofer diffraction theory can be employed to interpret the far-field radiation pattern, which can be given by[18]

$$Far(\theta) = I(\theta)G(\theta), \tag{4}$$

with

$$G(\theta) = \left| \sum_{l=1}^{N} P_l \exp(ik_0 d sin\theta) \right|^2, \tag{5}$$

where $I(\theta)$ is far-field pattern of individual laser; $G(\theta)$ is called grating function; P_l are admixture factors, E_l/E_1; d is the center-to-center spacing of adjacent lasers; θ is the angle in the reference plane; k_0 is the value of wave vector for free-space wavelength. For the in-phase mode, because all lasers have the same phases, the admixture factors P_l are all equal to one. The equation (4) shows that the far-field radiation pattern is influenced by two effects, $I(\theta)$ and $G(\theta)$. The $I(\theta)$ is far-field radiation pattern of each individual lasers, which is mainly a result of single-slit diffraction effect and the $G(\theta)$ represents the multiple-slits interference effect. The separation between adjacent peaks $\delta\theta$ is mainly dependent on the $G(\theta)$, the interference effect, which is given by

$$dsin\delta\theta = \lambda, \tag{6}$$

where d is center-to-center spacing of adjacent lasers, so the value of $\delta\theta$ is 10.6°. This is very close to the experiment results. The solid curve in the Figure 5 is simulated far-field pattern of three Gaussian sources with same optical phase (in-phase mode). The simulated curve fits very well with the measured far-field data. This indicates that phase-locked behavior among the lasers array is achieved and in-phase mode operation is taken.

We also fabricated devices with length of Talbot cavity $Z_t/2$. Measured far-field radiation patterns of such devices at different injection currents are shown in figure 5b. Two peaks locate at 5.2° and -5.2° respectively, and FWHM of each peak is about 4°. The solid curve in the Figure 5b is simulated far-field of out-of-phase mode. It reflects that out-of-phase mode operation is taken at this case. What we must notice is that the two peaks have opposite optical phases. Because the maximum intensity of the far-field is not in the center, such mode operation is often not desired for practical applications.

In summary, we have demonstrated a new coupling scheme to achieve phase-locked arrays of mid-infrared QCLs, diffraction coupled phase-locked arrays. Phase-locked behavior is achieved by integrating a Talbot cavity to adjust total optical losses of each mode. The in-phase mode operation can be achieved by controlling the length of Talbot cavity to be $Z_t/4$, where the in-phase mode has the lowest total optical losses and is selected. The

far-field radiation patterns indicate that near diffraction-limited beam quality has been achieved. The far-field radiation patterns can be well predicted and explained by the multi-slits Fraunhofer diffraction theoretical model. The in-phase mode operation shows high modal stability because of much smaller optical loss than those of other supermodes.

This work was supported by the National Basic Research Program of China (Grant Nos. 2013CB632801), National Key Research and Development Program (Grant Nos. 2016YFB0402303), National Natural Science Foundation of China (Grant Nos. 61435014, 61627822, 61574136, 61306058), Key Projects of Chinese Academy of Sciences (Grant No. ZDRW-XH-2016-4), and Beijing Natural Science Foundation (Grant No. 4162060).

[1] C. Gmachl, F. Capasso, D. L. Sivco, and A. Y. Cho, Rep. Prog. Phys. **64**, 1533 (2001).
[2] J. Faist, F. Capasso, D. L. Sivco, C. Sirtori, A. L. Hutchinson, and A. Y. Cho, Science **264**, 553 (1994).
[3] Y. Yao, A. J. Hoffman, and C. F. Gmachl, Nat. Photonics **6**, 432 (2012).
[4] Y. Bai, S. R. Darvish, S. Slivken, P. Sung, J. Nguyen, A. Evans, W. Zhang, and M. Razeghi, Appl. Phys. Lett. **91**, 141123 (2007).
[5] P. Rauter, S. Menzel, A. K. Goyal, B. Gokden, C. A. Wang, A. Sanchez, G. W. Turner, and F. Capasso, Appl. Phys. Lett. **101**, 261117 (2012).
[6] Y. Bai, S. Slivken, Q. Lu, N. Bandyopadhyay, and M. Razeghi, Appl. Phys. Lett. **101**, 081106 (2012).
[7] S. Ahn, C. Schwarzer, T. Zederbauer, D. C. MacFarland, H. Detz, A. M. Andrews, W. Schrenk, and G. Strasser, Appl. Phys. Lett. **104**, 051101 (2014).
[8] D. Botez and D. R. Scifres, *Diode Laser Arrays* (Cambridge University Press, 1994).
[9] G. M. de Naurois, M. Carras, B. Simozrag, O. Patard, F. Alexandre, and X. Marcadet, AIP Adv. **1**, 032165 (2011).
[10] Y. H. Liu, J. C. Zhang, F. L. Yan, F. Q. Liu, N. Zhuo, L. J. Wang, J. Q. Liu, and Z. G. Wang, Appl. Phys. Lett. **106**, 142104 (2015).
[11] J. D. Kirch, C. C. Chang, C. Boyle, L. J. Mawst, D. Lindberg, T. Earles, and D. Botez, Appl. Phys. Lett. **106**, 061113 (2015).
[12] T. Y. Kao, Q. Hu, and J. L. Reno, Appl. Phys. Lett. **96**, 101106 (2010).
[13] L. K. Hoffmann, C. A. Hurni, S. Schartner, M. Austerer, E. Mujagic, M. Nobile, A. Benz, W. Schrenk, A. M. Andrews, P. Klang, and G. Strasser, Appl. Phys. Lett. **91**, 161106 (2007).
[14] J. M. Wen, Y. Zhang, and M. Xiao, Adv. Opt. Photon. **5**, 83 (2013).
[15] J. Z. Wilcox, M. Jansen, J. J. Yang, S. S. Ou, M. Sergant, and W. W. Simmons, Appl. Phys. Lett. **50**, 1319 (1987).
[16] D. G. Hall, R. R. Rice, and J. D. Zino, Opt. Lett. **4**, 292 (1979).
[17] J. C. Zhang, F. Q. Liu, S. Tan, D. Y. Yao, L. J. Wang, L. Li, J. Q. Liu, and Z. G. Wang, Appl. Phys. Lett. **100**, 112105 (2012).
[18] E. Kapon, J. Katz, and A. Yariv, Opt. Lett. **9**, 125 (1984).